Chapter 10

Condensate Drop Movement by Surface Temperature Gradient on Heat Transfer Surface in Marangoni Dropwise Condensation

Yoshio Utaka and Zhihao Chen

Additional information is available at the end of the chapter

http://dx.doi.org/10.5772/51830

1. Introduction

Marangoni dropwise condensation occurs in the condensation of a binary vapor mixture of a positive system, in which the surface tension of the mixture has a negative gradient with the mass fraction of the more volatile component, such as water–ethanol and water–ammonium mixtures. Thick condensate areas have higher liquid surface temperatures than thin areas; therefore, the surface tension flow is induced toward the peak of the condensate from thinner areas as a result of the vapor–liquid equilibrium and the variation in the surface tension in the binary vapor condensation of a positive system. This phenomenon differs essentially from so-called dropwise condensation on a hydrophobic surface, because there is a continuous thin liquid film between condensate drops and condensation occurs on a hydrophilic surface. This phenomenon was first reported by Mirkovich and Missen [1] in 1961 for a binary mixture of organic vapors. Ford and Missen [2] demonstrated that the criterion for instability of a condensate liquid film is $d\sigma/db > 0$, where b denotes the condensate film thickness. Fujii et al. [3] conducted an experimental investigation of the condensation of water–ethanol mixtures on a horizontal tube and observed several different condensation modes dependent on the concentration. Morrison and Deans measured the heat transfer characteristics of a water–ammonium vapor mixture and found that it exhibited enhanced heat transfer [4].

In recent years, Utaka and co-workers conducted research [5–9] on the dominant factors (surface subcooling, vapor mass fraction, and vapor velocity) in determining the condensation modes and heat transfer characteristics of Marangoni condensation. The

major results on the heat transfer characteristics of Marangoni condensation were summarized in reference 9. Heat transfer was significantly enhanced for a low mass fraction of ethanol in a water–ethanol mixture. Murase et al. [10] studied Marangoni condensation of steam–ethanol mixtures using a horizontal condenser tube, and the results exhibited similar trends to those obtained by Utaka and Wang [7] for vertical surfaces.

The mechanisms of Marangoni condensation have also been studied. Hijikata et al. [11] presented a theoretical drop growth mechanism for Marangoni dropwise condensation. That is, the Marangoni effect occurs due to the surface tension difference which plays a more important role than the surface tension. Akiyama et al. [12] performed a 2-dimensional numerical simulation of the condensation of water-ethanol vapor on a horizontal heat transfer surface and found a 2 K temperature difference between the condensate film area and the crest of the condensate drop. Marangoni flow occurs in a condensate liquid and is driven by the surface tension gradient induced by the temperature difference. Utaka et al. [13] investigated the effect of the initial drop distance, which is the average distance between initially formed drops grown from a thin flat condensate film that forms immediately after a drop departs. They clarified that the initial drop distance is closely related to the heat transfer characteristics of Marangoni condensation. Furthermore, Utaka and Nishikawa [14] measured the thickness of condensate films on the tracks of departing drops and between drops using the laser extinction method, in which the proportion of laser light absorbed by the condensate liquid is dependent on the liquid thickness. The condensate film was approximately 1 μm thick and was strongly dependent on the initial drop distance and the heat transfer characteristics.

Marangoni condensation occurs due to the instability of Marangoni force acting on the condensate film. Condensate drops move spontaneously without any external forces when a bulk temperature gradient is applied to a horizontal heat transfer surface, only due to the imbalance of the surface tension distribution around the drops. This kind of phenomena could also occur in a low-gravity environment. This implies that condensate drops can be moved by applying a bulk surface temperature to a heat transfer surface. It is thus possible to remove a thick liquid film and large condensate drops by exploiting this spontaneous movement of condensate drops. A highly efficient heat exchanger could then be realized. Moreover, since non-uniform temperature distributions are often generated in heat exchangers, it is essential to clarify the heat transfer and condensate movement characteristics in Marangoni condensation when there is a temperature distribution on the heat transfer surface. It is also considered that the circulation of condensate driven by surface tension flow could be utilized in some heat transfer devices (e.g., a wickless heat pipe). Utaka and Kamiyama [15] examined the effect of the bulk surface tension gradient on condensate drop movement when a steady bulk temperature gradient was applied to horizontal and inclined heat transfer surfaces in the condensation

of a water–ethanol vapor mixture. The condensate drops moved from the low-temperature side to the high-temperature side. The drop velocity increased with the surface tension gradient on the condensing surface and was independent of the drop size. Chen and Utaka [16] investigated the mechanisms and characteristics of drop movement on a horizontal condensing surface with a bulk temperature gradient for Marangoni dropwise condensation of a water–ethanol vapor mixture. In particular, experimental observations and measurements on the dominant factors affecting condensate drop movement were conducted, such as 1) bulk surface tension gradient, and 2) initial drop distance (adopted as a parameter for the Marangoni force and the condensate drop shape). The velocity of condensate drop movement was determined to correlate well with both the surface tension gradient and the initial drop distance.

In this chapter, the characteristics and mechanisms of condensate drop movement driven by a surface tension gradient in Marangoni dropwise condensation are summarized on the basis of the presented researches.

2. Marangoni dropwise condensation

2.1. Heat transfer characteristics in Marangoni dropwise condensation

In the condensation of a binary vapor mixture, such as water–ethanol vapor, the Marangoni force (indicated by the arrows in Fig. 1) pulls the condensate liquid from the periphery toward the peak along the surface of a condensate drop, whereby dropwise condensation occurs. The Marangoni force here is the driving force for condensate flow, which is considered to be caused by a surface tension difference on the condensate surface, based on the vapor–liquid equilibrium and the variation in the surface tension for a water–ethanol liquid mixture (see Fig. 2). This kind of phenomenon is referred to as 'Marangoni dropwise condensation'.

Utaka and Terachi [6] and Utaka and Wang [7] reported that significantly enhanced heat transfer could be realized by decreasing the thermal resistance of the condensate liquid in the Marangoni dropwise condensation of a water–ethanol vapor mixture. Utaka and Terachi [6] measured the condensation characteristics and clarified that surface subcooling is one of the dominant factors that determines the condensate and heat transfer characteristics of Marangoni condensation. More accurate measurements of a wider range of ethanol mass fraction and surface subcooling were conducted by Utaka and Wang [7], some of the results of which are shown in Fig. 3 and Fig. 4. Figure 3 shows the heat transfer coefficient of Marangoni condensation for water–ethanol vapor mixtures with various ethanol mass fractions. Figure 4 shows the variation in the ratio of the peak heat transfer coefficient of the mixture vapor to that of pure steam. These two figures indicate that the condensation heat transfer is significantly enhanced by the addition of an extremely small amount of ethanol and the heat transfer coefficient of the vapor mixture is approximately 8 times higher than that of pure steam.

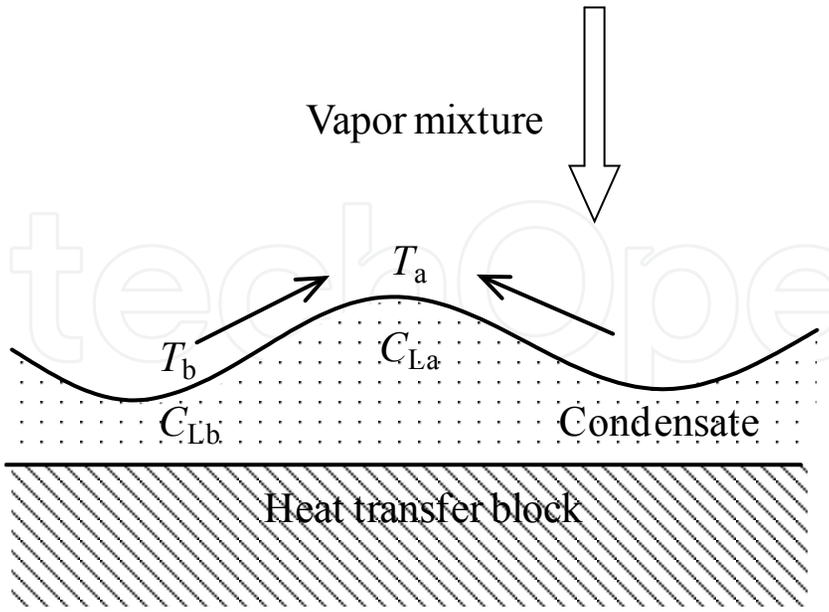

Figure 1. Mechanism for Marangoni dropwise condensation

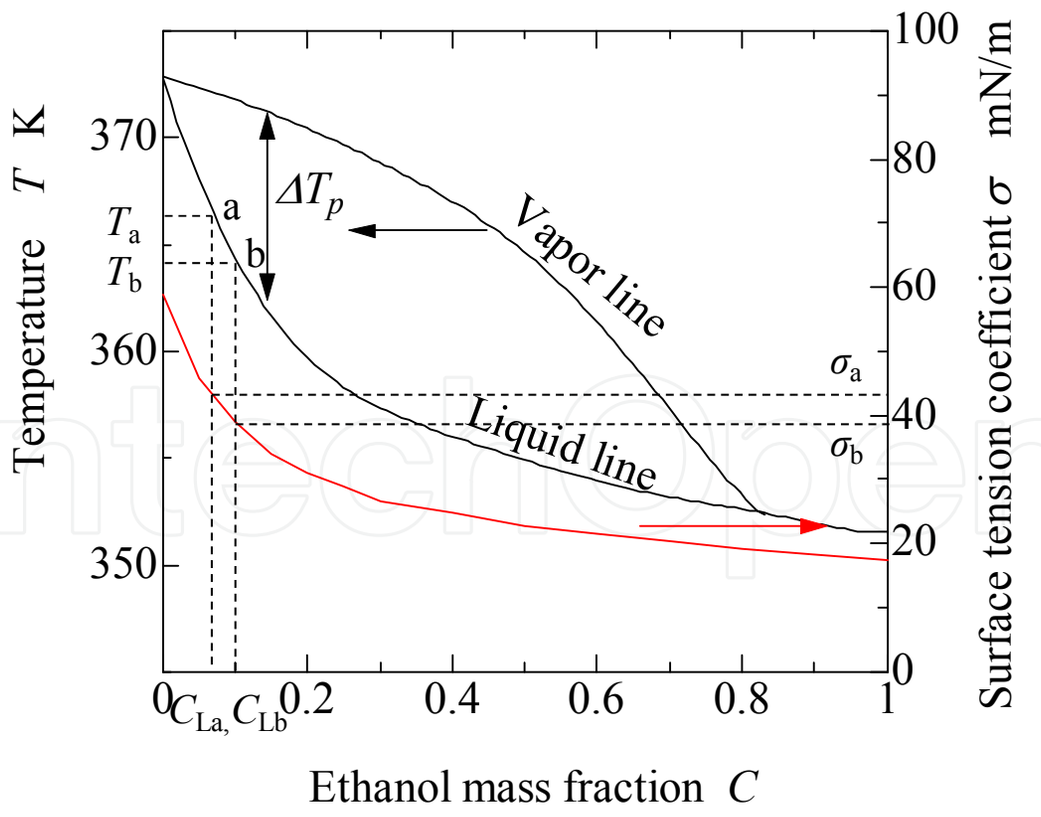

Figure 2. Vapor–liquid equilibrium and variation of surface tension coefficient for water–ethanol mixture

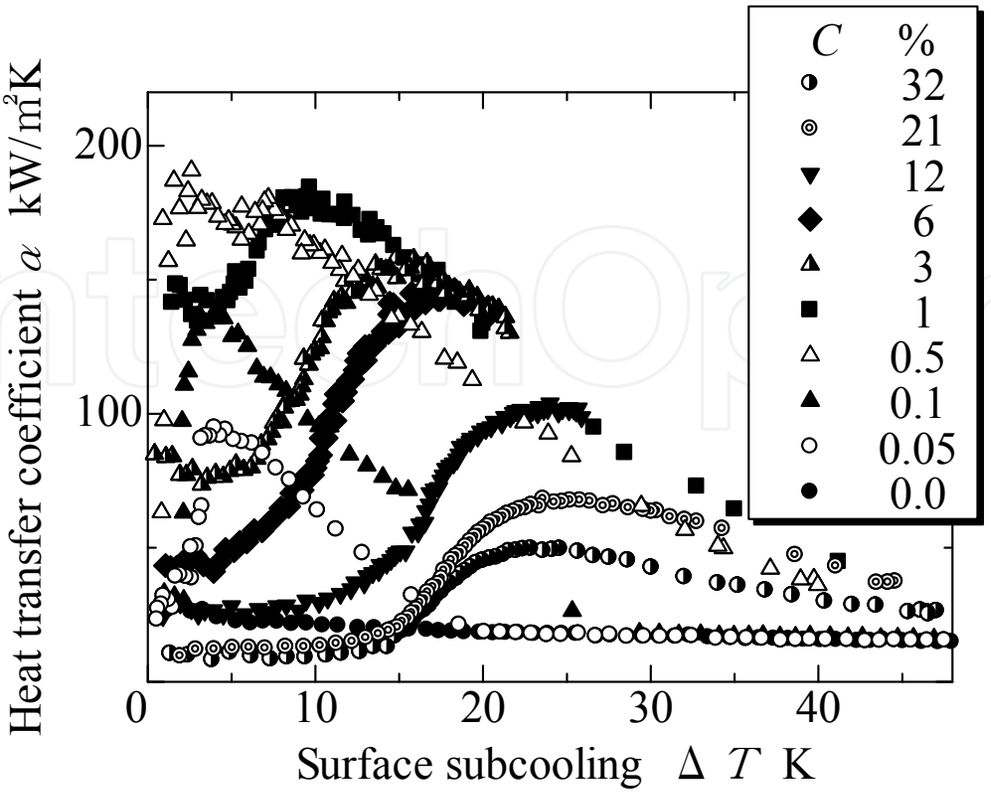

Figure 3. Condensation characteristics of water–ethanol vapor mixtures with various ethanol mass fractions

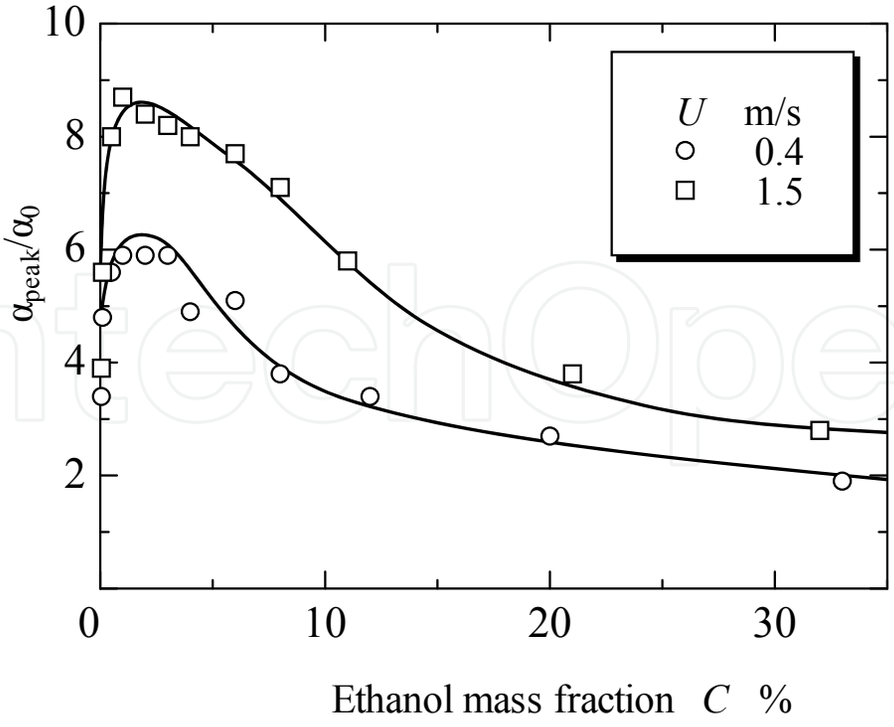

Figure 4. Variation in the ratio of the peak heat transfer coefficient of the vapor mixture to that of pure steam

2.2. Relations among initial drop distance, Marangoni force and shape (angle) of condensate drop

In Marangoni dropwise condensation, small condensate drops initially form from a smooth and thin liquid film adjacent to the periphery of a large condensate drop after its departure. Figure 5 shows time-series microscopic images of the formation of small condensate drops. These initially formed drops are called initial drops and the average distance between the centers of the initial drops is defined as the initial drop distance.

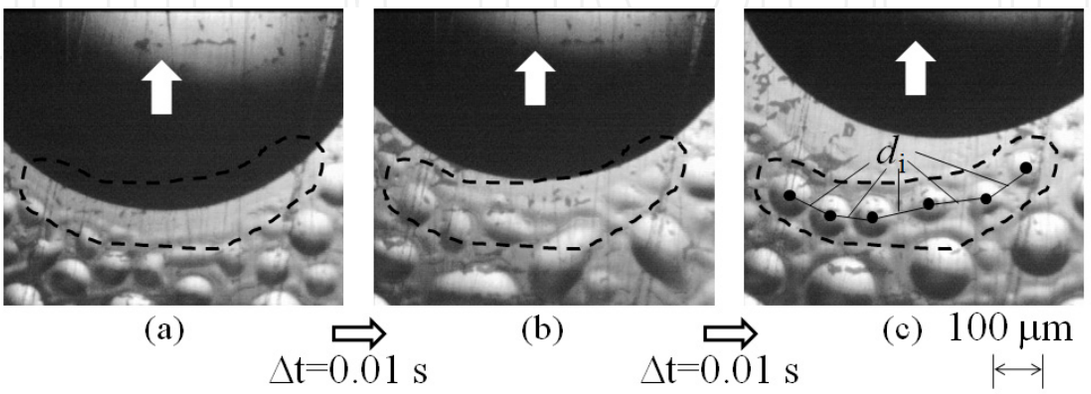

Figure 5. Initial drop formation process with initial drop distance (d_i) indicated

Condensate drops form in Marangoni dropwise condensation due to the Marangoni force acting on the surface of the condensate liquid. Therefore, the Marangoni force is considered to be closely related to the heat transfer mechanisms of Marangoni dropwise condensation. It is also reasonable that the formation of initial drops and the initial drop distance is determined by the strength of the Marangoni force. Thus, a close correlation exists between the initial drop distance and Marangoni force. Consequently, the initial drop distance is adopted as an important parameter of the heat transfer characteristics and mechanisms of Marangoni condensation in the studies of Utaka et al. [13] and Utaka and Nishikawa [14]. Figures 6(a) and (b) show respective plots of the heat transfer coefficient and the initial drop distance as a function of surface subcooling based on data measured by Utaka et al. [13]. The initial drop distances have U-shaped curves with minima that correspond to distances in the range 30–150 μm, depending on the surface subcooling and the mass fraction of ethanol. Surface subcooling at the minimum initial drop distances coincides with that at the maximum heat transfer coefficient. Utaka and Nishikawa [14] investigated the relationship between the liquid film thickness and the initial drop distance (Fig. 7) for a water–ethanol mixture using the laser extinction method. A condensate liquid film of approximately 1 μm thickness remained after sweeping by departing drops and between condensate drops. The minimum condensate film thickness decreased with initial drop distance for surface subcooling lower than the maximum heat transfer point, even when the condensation rate increased.

These two studies demonstrated that there is a close relationship between the heat transfer coefficient and characteristic parameters such as the initial drop distance and the minimum condensate thickness. In the surface subcooling region near the maximum heat transfer coefficient, the initial drop distance and minimum film thickness tend to assume minimum

values as a result of the driving force being a maximum, due to the surface tension gradient on the condensate surface. Thus, when the initial drop distance decreases, heat transfer is enhanced by thinning of the condensate film that could result in a reduction in the thermal resistance of the condensate. In addition, the condensate drop shape changes with increasing Marangoni force and the condensate film becomes thinner, even when condensation rate increases. This implies that the drop height increases as the drops approach hemispherical shapes due to an increase in the Marangoni force. The correlation among the Marangoni force, initial drop distance and shape (angle) of condensate drops, as

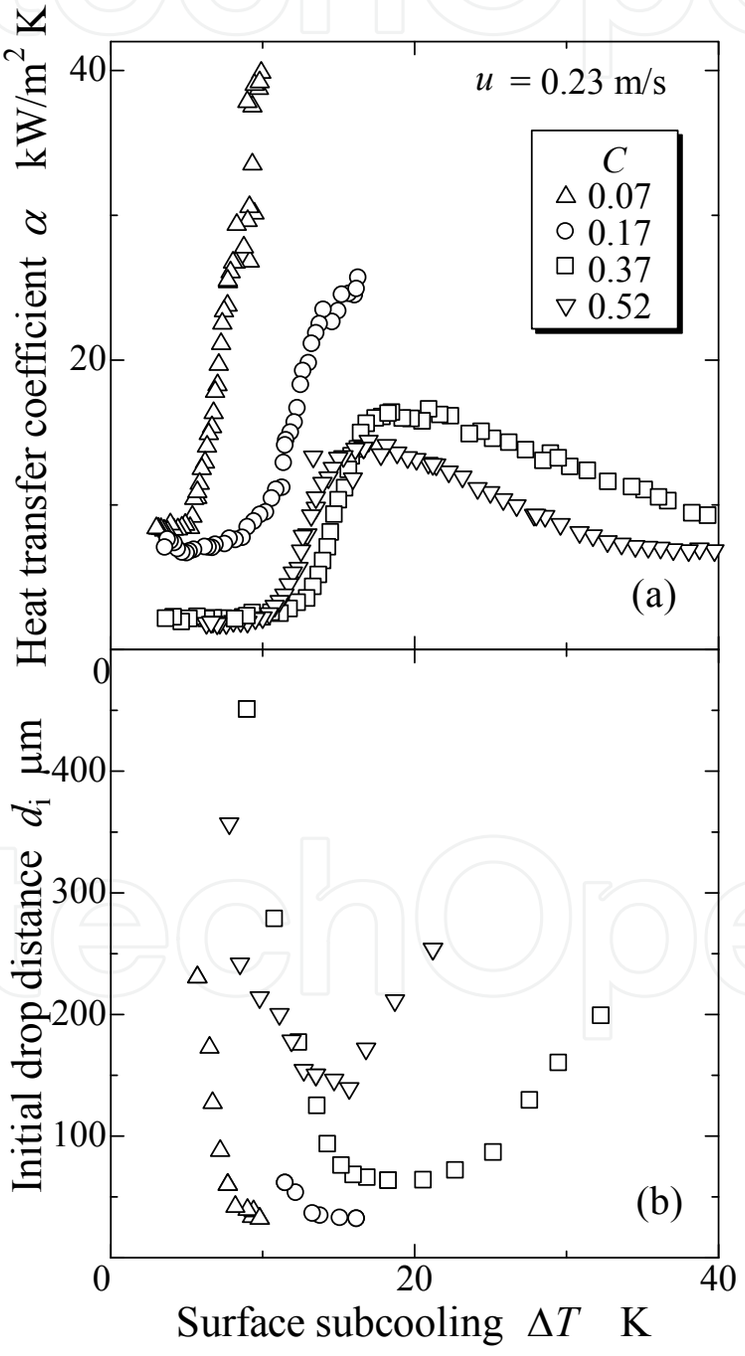

Figure 6. Variation of heat transfer coefficient and initial drop distance as a function of surface subcooling

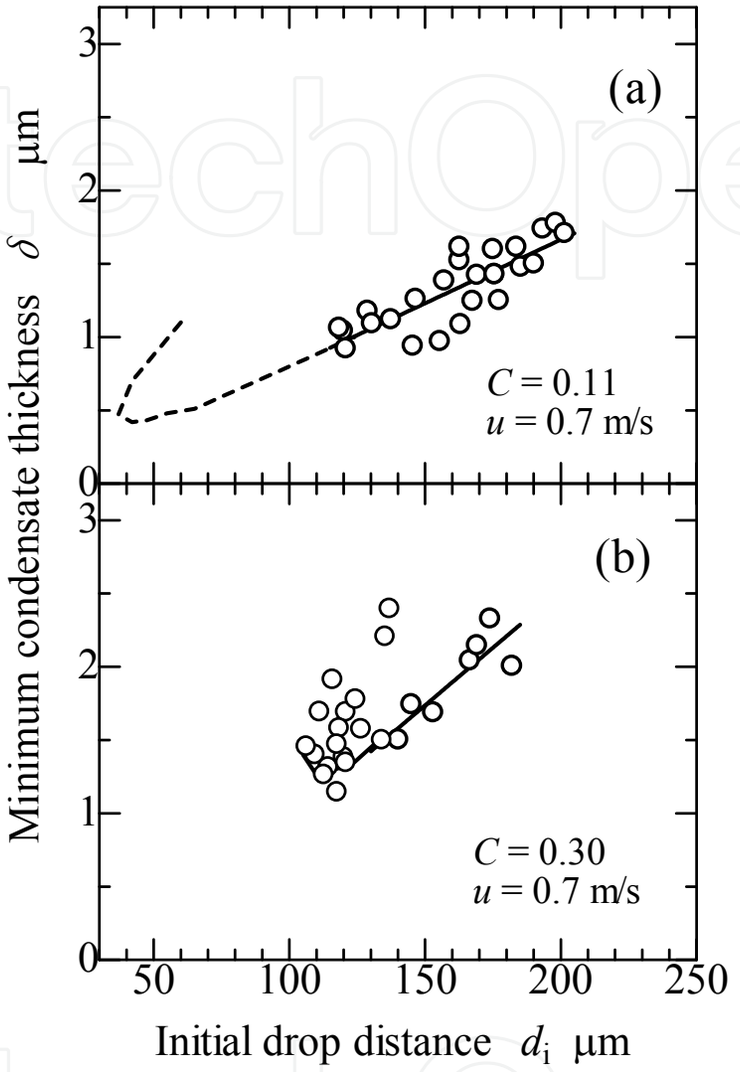

Figure 7. Variation of minimum condensate film thickness as a function of initial drop distance

shown in Fig. 8, could be inferred on the basis of these experimental results. For certain mass fractions of ethanol, the experimental condition of surface subcooling determines the strength of the Marangoni force, and thus the initial drop distance and shape of the condensate drop are also determined. Therefore, if any one of the three factors is known, the two other factors can be determined based on the corresponding correlations. The qualitative correlations are inferred from the experimental results. The quantitative correlations were experimentally studied and are introduced in the following section.

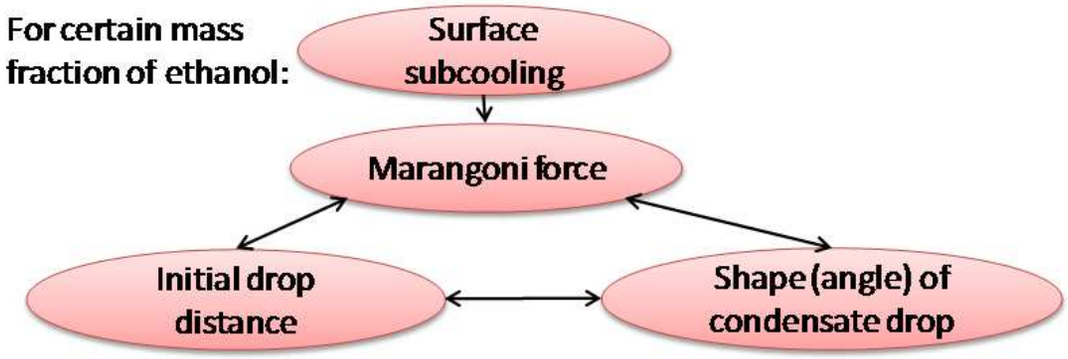

Figure 8. Correlation between Marangoni force, initial drop distance and condensate drop shape

3. Spontaneous movement of condensate drops in Marangoni dropwise condensation

When a bulk temperature gradient is applied to a horizontal heat transfer surface or in a low-gravity environment under a Marangoni condensation field, condensate drops move spontaneously without external forces. The reason for condensate drop movement is considered to be as follows. A Marangoni force (F_H or F_L in Fig. 9, the letter 'H' represents the high temperature side and 'L' represents the high temperature side.) is induced by the difference in surface tension on the condensate surface in Marangoni dropwise condensation. The condensate near the periphery of a condensate drop is pulled along the condensate liquid surface toward the peak of the drop. A reactive force against the surface tension flow caused by the Marangoni force is induced at the drop periphery. When there is no bulk temperature gradient, the reactive force is uniform around the drop periphery and averages out over time, so that the drop does not move to a large extent. In contrast, when a bulk temperature gradient is applied to a horizontal heat transfer surface, the horizontal component of the reactive force (F_{HX} or F_{LX} in Fig. 9, the letter 'X' represents the horizontal component.) around a condensate drop becomes nonuniform, as shown in Fig. 9. Consequently, condensate drops move spontaneously on the heat transfer surface without external forces.

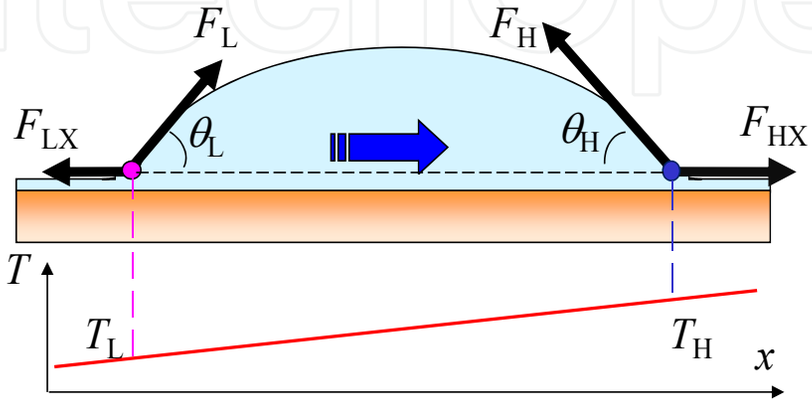

Figure 9. Schematic diagram of the driving force for condensate drop movement

It is considered that the imbalance of the reactive force is determined by the bulk surface tension gradient of the condensate liquid. Consequently, the velocity of condensate drop movement is considered to be affected by the bulk surface tension gradient. The bulk surface tension gradient is calculated from the surface tension difference, which corresponds to the time-averaged surface temperature distribution of the extremely thin liquid film covering the heat transfer surface. The horizontal component of the Marangoni force depends on the overall magnitude of the Marangoni force and the shape (angle) of the condensate drop. Therefore, it is conceivable that the movement of the condensate drop is also determined by these two factors. Based on the correlation between the Marangoni force, initial drop distance and the angle of the condensate drop shown in Fig. 8, it follows that condensate drop movement is also affected by these three factors. Utaka and co-workers [15, 16] have focused on these factors and carried out several experimental and numerical studies on the characteristics and mechanisms of condensate drop movement in Marangoni dropwise condensation.

3.1. Experimental apparatus

Figure 10 shows a schematic of a typical experimental system. A vapor mixture is generated by electrically heating a water–ethanol mixture with a certain mass fraction in a vapor generator. The vapor is partially condensed on a heat transfer block, and is almost completely condensed in an auxiliary condenser after passing through the condensing chamber. The vapor pressure is maintained close to atmospheric pressure by a small opening to the atmosphere between the auxiliary condenser and condensate receiver. The condensate is fed back into the vapor generator after deaeration to remove non-condensable gases dissolved in the condensate. In addition, the vapor is made to flow in the opposite direction to the condensate drop movement to distinguish the driving force of drop movement from the shear force of the vapor flow. Figure 11 shows a schematic of the condensing chamber, where the condensate drop behavior is observed through front and side windows.

Figure 12 shows a schematic of the heat transfer block, which was made of brass with a surface area of 20×20 mm^2 that was positioned horizontally for the experiments. A triangular cross-section of constantan, which has low thermal conductivity, was soldered onto the cooling surface of the heat transfer block. This allowed a bulk temperature gradient to be applied to the heat transfer surface by uniformly cooling the constantan surface with multiple water jet spray. Temperature was measured using thermocouples located inside the heat transfer block, and the surface temperature distribution was determined by two-dimensional extrapolation. The heat transfer surface was coated with titanium dioxide to make it hydrophilic to distinguish it from dropwise condensation on a hydrophobic surface. Experiments were conducted continuously using quasi-steady-state measurements, in which the temperature of the cooling water was changed very slowly.

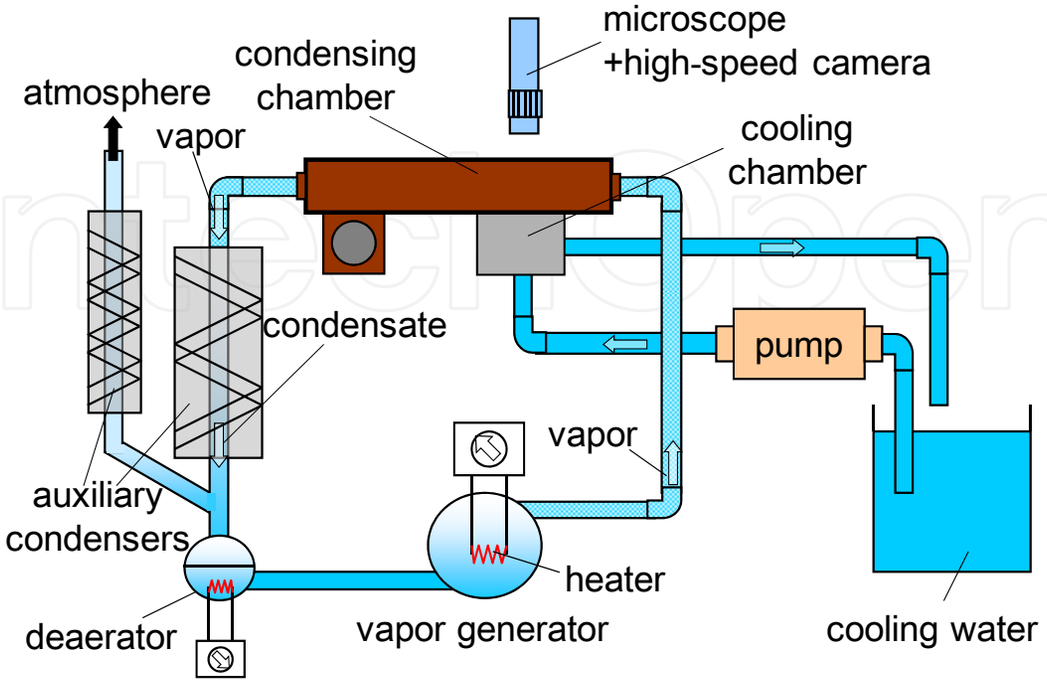

Figure 10. Schematic of a typical experimental apparatus setup

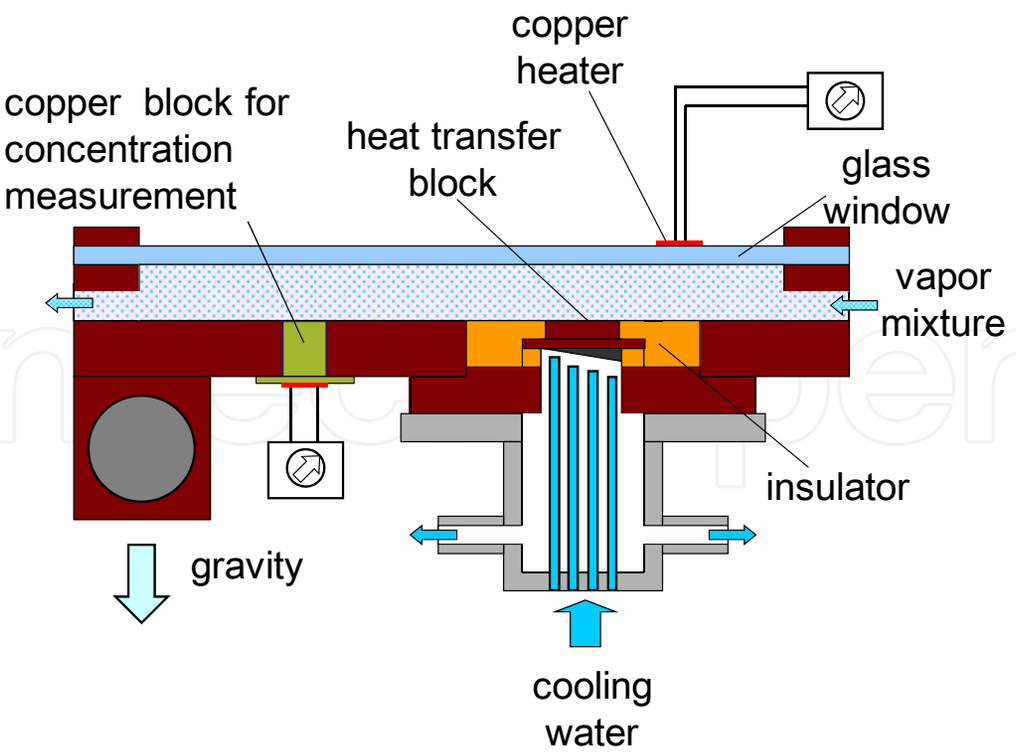

Figure 11. Schematic of the condensing chamber

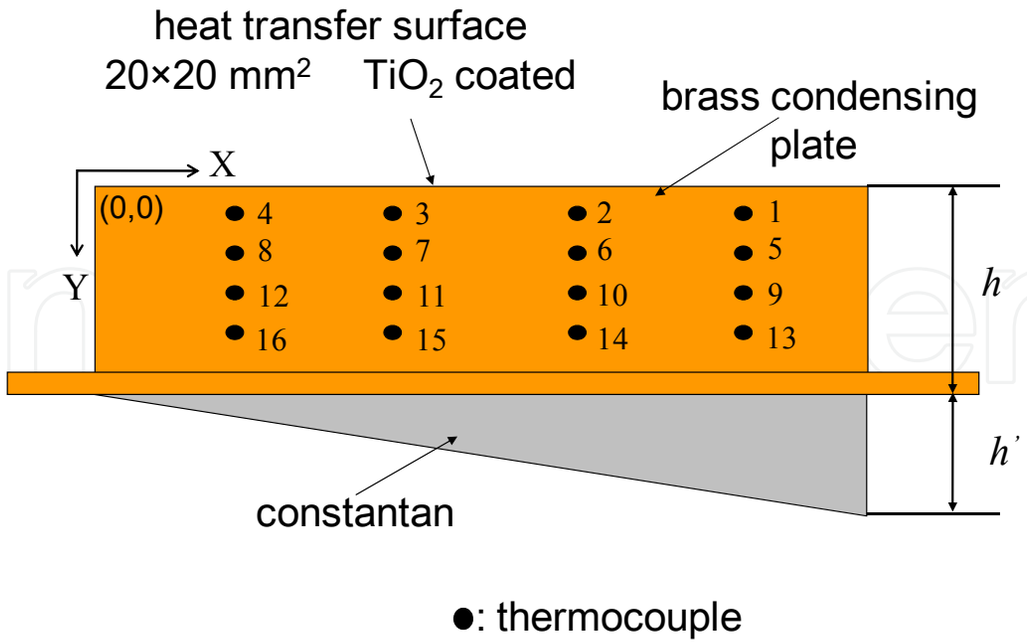

Figure 12. Schematic of the heat transfer block

3.2. Variations of condensate drop shape, initial drop distance and heat transfer coefficient against surface subcooling

To confirm the correlations among the Marangoni force, initial drop distance and shape of condensate inferred in section 2.2, experimental studies were conducted to investigate the quantitative relations. The angle of the condensate drop, initial drop distance and heat transfer coefficient were experimentally measured and the relations are discussed. A profile image of a condensate drop taken through the side view window is shown in Fig. 13. Vapor flows from the right side to the left side, which is the high-temperature side of the heat transfer surface, as does the condensate drop. The angle between the surface of the condensate drop and the heat transfer surface near the drop base as shown in the profile image is defined as the angle of the condensate drop. The angle in the direction of forward movement is the advancing angle θ_a, and that at the opposite side is the receding angle, θ_r. Since similar tendencies in the variation of advancing and receding angles were observed, an average value of the advancing and receding angle for single condensate drops was calculated. The variation of average condensate drop angle, initial drop distance and the heat transfer coefficient as a function of surface subcooling are shown in Fig. 14.

Several tendencies are evident in Fig. 14. For each mass fraction of ethanol, as with the previous results, the heat transfer coefficient increases and the initial drop distance decreases with increasing surface subcooling. In addition, the average condensate drop angle increases with increasing surface subcooling. This indicates that the decrease in the initial drop distance corresponds to an increase in the angle of the condensate drop. The maximum average angle of a condensate drop was approximately 35-45°, which is slightly

smaller than the typical contact angle of a condensate drop on a hydrophobic surface. Moreover, for the same surface subcooling, a higher heat transfer coefficient and smaller initial drop distance were realized for a smaller mass fraction of ethanol.

The experimental results indicate that greater surface subcooling or lower mass fraction of ethanol gives a smaller initial drop distance, and the average angle of the condensate drop is larger due to the stronger Marangoni force. Therefore, it was confirmed that the three main factors have quantitative correlations. In addition, there was a large amount of scatter in the data for the condensate drop angle, which is caused by frequent coalescence when the drops are moving or by variation of the temperature distribution on the heat transfer surface. This scatter is considered to be an essential characteristic of Marangoni dropwise condensation. Therefore, in the three important factors, the Marangoni force cannot be measured and the condensate drop angle has large amount of scatter. In contrast with the other two factors, initial drops grow from a thin flat condensate film that appears immediately after a drop departs, the state before the initial drops form is relatively stable, and thus, the measurement of the initial drop distance has good repeatability. Therefore, it is appropriate to adopt the initial drop distance as the dominant parameter of Marangoni dropwise condensation that represents the Marangoni force and the shape of a condensate drop.

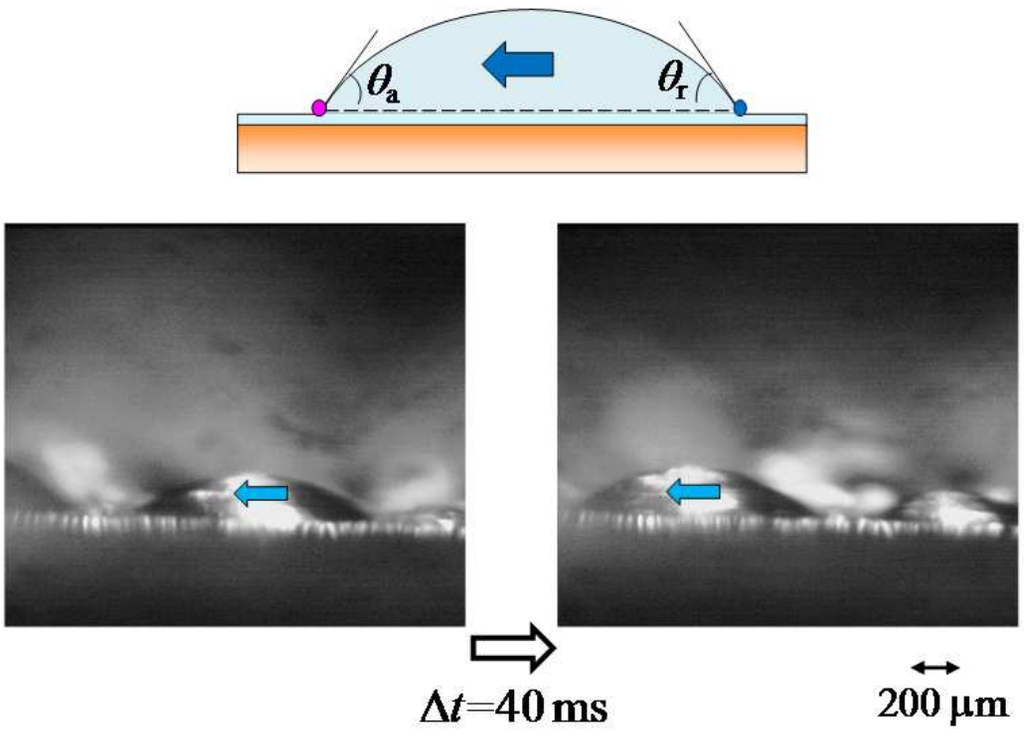

Figure 13. Profile image of condensate drop shape

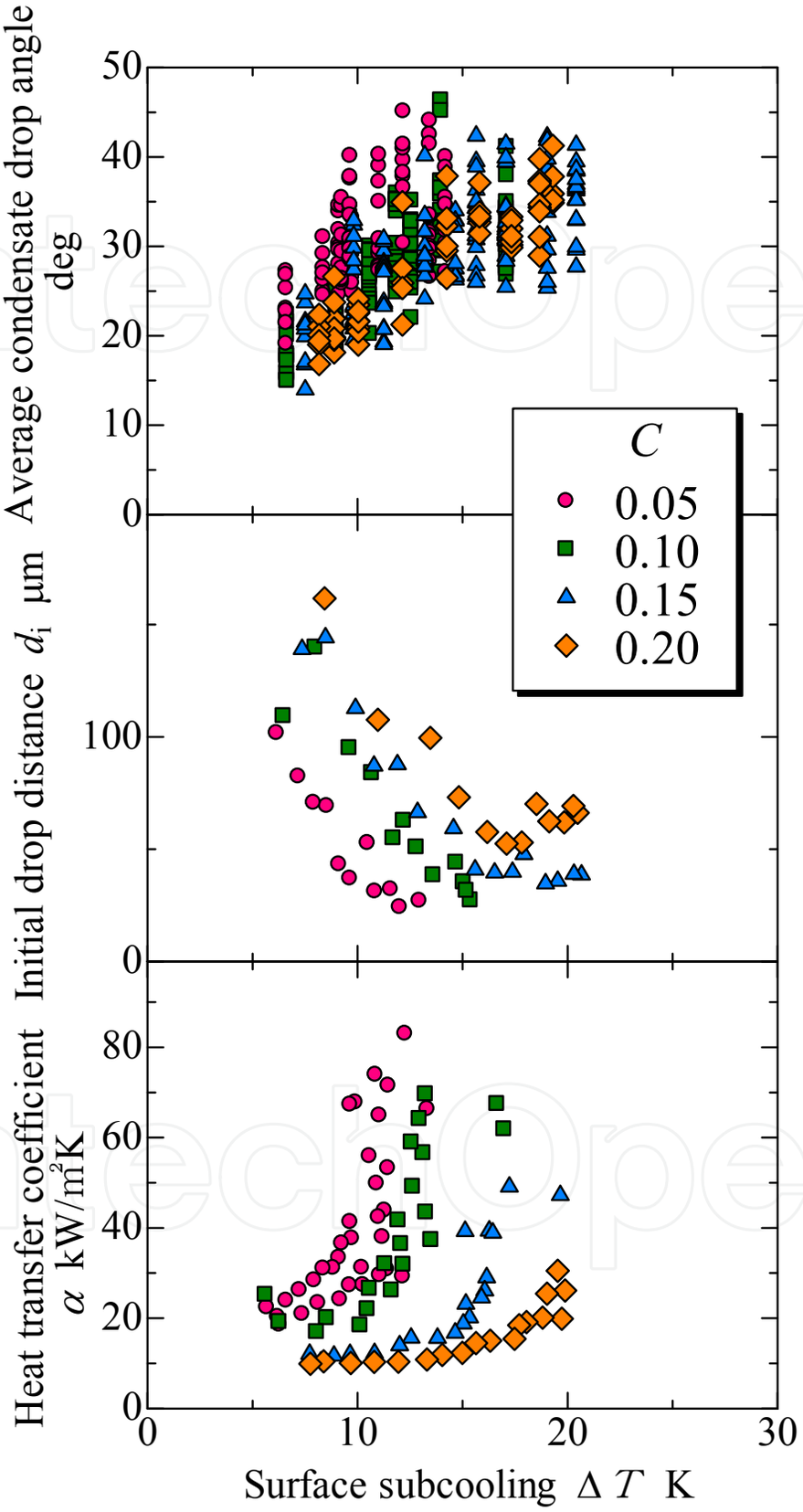

Figure 14. Variation of condensate drop angle, initial drop distance and heat transfer coefficient as a function of surface subcooling for various mass fractions of ethanol

3.3. Effect of bulk surface tension gradient on velocity of drop movement

Utaka and Kamiyama [15] examined the effect of the bulk surface tension gradient on condensate drop movement when a steady bulk temperature gradient was applied to horizontal and inclined heat transfer surfaces during the condensation of a water–ethanol vapor mixture. Figure 15 shows images of condensate drop movement on the horizontal heat transfer surface. The upper part of the image is the high-temperature side and the lower part is the low-temperature side. The condensate drops move from the low-temperature side to the high-temperature side. The variations of condensate drop velocity are shown for various ethanol mass fractions as a function of the bulk surface tension gradient in Fig. 16. The drop velocity increased with increasing surface tension gradient on the condensing surface and was independent of the drop size. Moreover, although there is a large scatter in the drop velocities due to frequent coalescence of the condensate drops, qualitatively similar tendencies of drop velocity were shown.

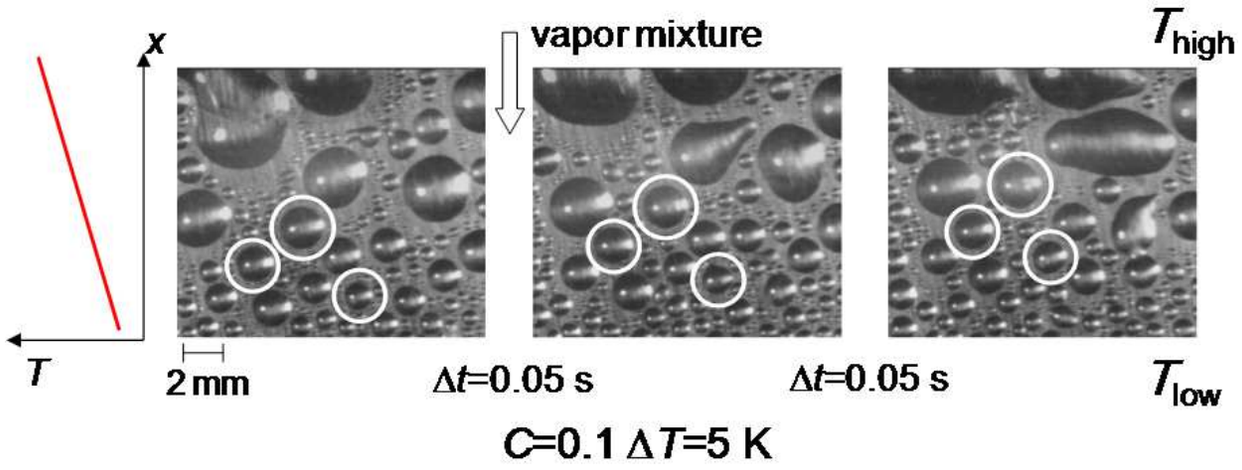

Figure 15. Appearance of condensate drop movement

3.4. Effect of initial drop distance on velocity of drop movement

Chen and Utaka [16] investigated the affects of the Marangoni force and the condensate drop angle on the velocity of condensate drop movement. As discussed in section 3.2, the initial drop distance was adopted as the dominant parameter representing the Marangoni force and angle of condensate drop. The variations of velocity of drop movement as functions of the initial drop distance and bulk surface tension gradient are shown in Figs. 17 and 18, respectively. The drop velocities vary significantly, so that an average velocity of all condensate drops was adopted for each set of conditions.

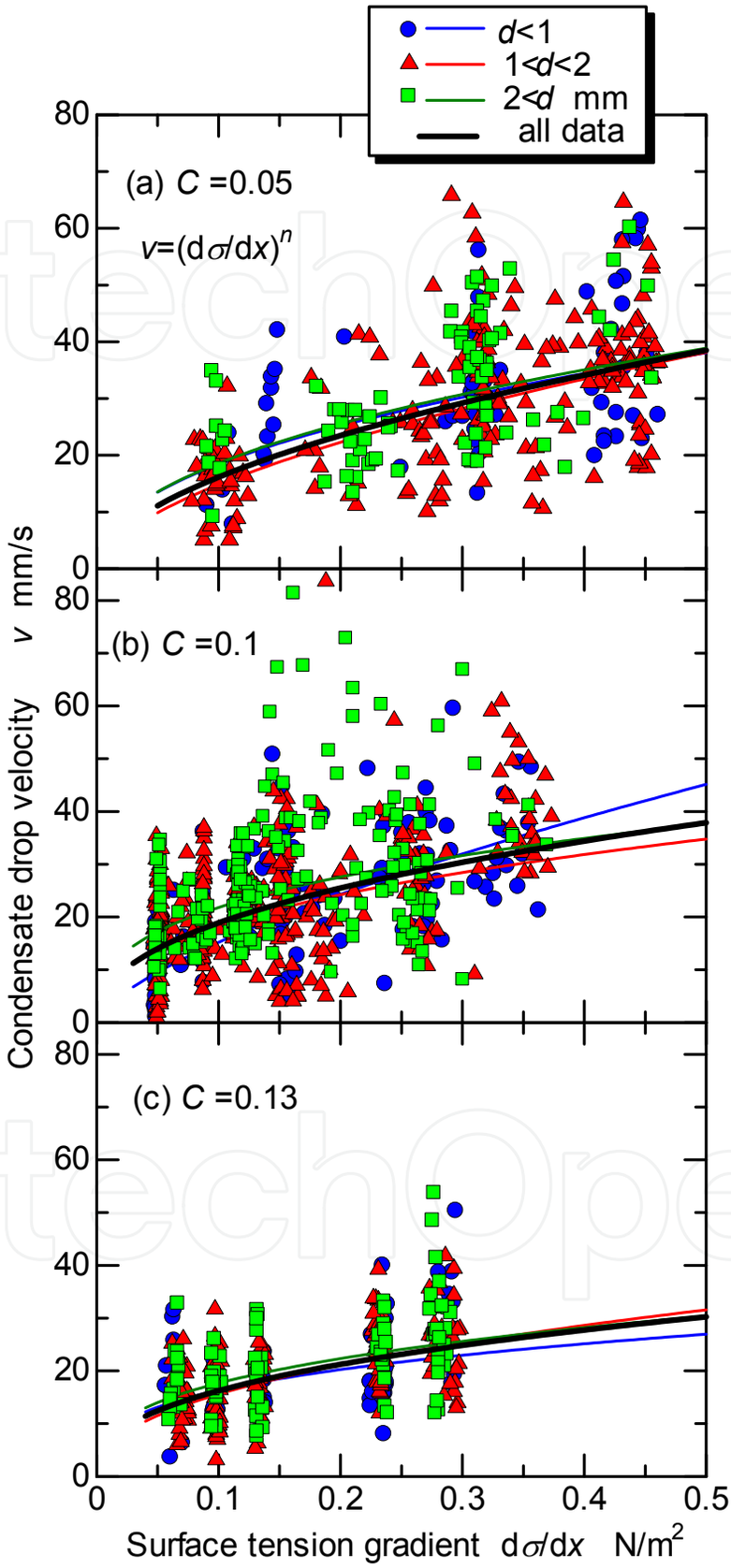

Figure 16. Variation of condensate drop velocity against bulk surface tension gradient

Figures 17 show plots of the average drop velocity as a function of the initial drop distance for ethanol mass fractions *C*, of 0.1, 0.15, 0.2, and 0.25 for six different bulk surface tension gradients. All experiments were performed in the surface subcooling range for which the heat transfer coefficient is less than its maximum value. Distinct trends between the average drop velocity and the initial drop distance are observed in Fig. 17. Qualitatively similar tendencies are evident and the curves have maximum values for each ethanol mass fraction and each surface tension gradient. When the initial drop distance decreases, the average drop velocity initially increases and then decreases after reaching a maximum value at almost the same surface tension gradient for all ethanol mass fractions. For example, for C = 0.15 and a bulk surface tension gradient of 0.2–0.3 N/m², the average drop velocity increases from v = 16 mm/s to a maximum value of v = 21 mm/s when the initial drop distance decreases from d_i = 190 to 130 μm. The average velocity then tended to decrease to v = 0 mm/s as d_i decreased to 25 μm. While the changes in drop velocity were gradual at relatively high bulk surface tension gradients, the drop velocities over the entire range of initial drop distances decreased significantly over a smaller range of bulk surface tension gradients for all ethanol mass fractions. Although it is not surprising that the driving force is approximately 0 at low surface tension gradients in the ranges –0.05 to 0 N/m² and 0–0.05 N/m² for all mass fractions, it is notable that the driving force is also very small for small d_i in the initial drop distance range of 30–40 μm, even at high surface tension gradients.

Figure 18 shows the effect of the bulk surface tension gradient on the drop velocity for four initial drop distances and for ethanol mass fractions *C*, of 0.1, 0.15, 0.2, and 0.25. Data with similar initial drop distances as those in Fig. 17 were selected and were plotted together and fitted with lines that pass through the origin. The drop velocity increases linearly with increasing bulk surface tension gradient for each initial drop distance range. Furthermore, the rate of increase in the drop velocity with the bulk surface tension gradient increases with increasing initial drop distance in the lower ranges of initial drop distance up to the peak average drop velocity shown in Fig. 17. Similar increasing rate were obtained in the larger ranges of initial drop distance for each mass fraction. The effect of the surface tension gradient on the drop velocity became stronger when the initial drop distance approached values that give rise to the maximum velocities shown in Fig. 17. For example, when the bulk surface tension gradient is –0.05 N/m², the velocity of condensate drops is around 0 mm/s when the initial drop distances are in the range of 30–35 μm. The velocity then increases with increasing bulk surface tension gradient; the velocity is 10 mm/s at a bulk surface tension gradient of 0.34 N/m². For larger initial drop distances, the increase in the drop velocity as a function of bulk surface tension gradient becomes more rapid when the initial drop distance was in the range of 60–80 μm. This increase becomes much more rapid and the velocity increases from 3.6 to 18.9 mm/s in the initial drop distance range of 155–255 μm, when the corresponding bulk surface tension gradient is increased from 0.09 to 0.28 N/m². For comparatively large initial drop distances in the ranges of 155–215 μm and 200–270 μm, the variations in the drop velocity as a function of the bulk surface tension gradient were similar, as shown in Fig. 18(b).

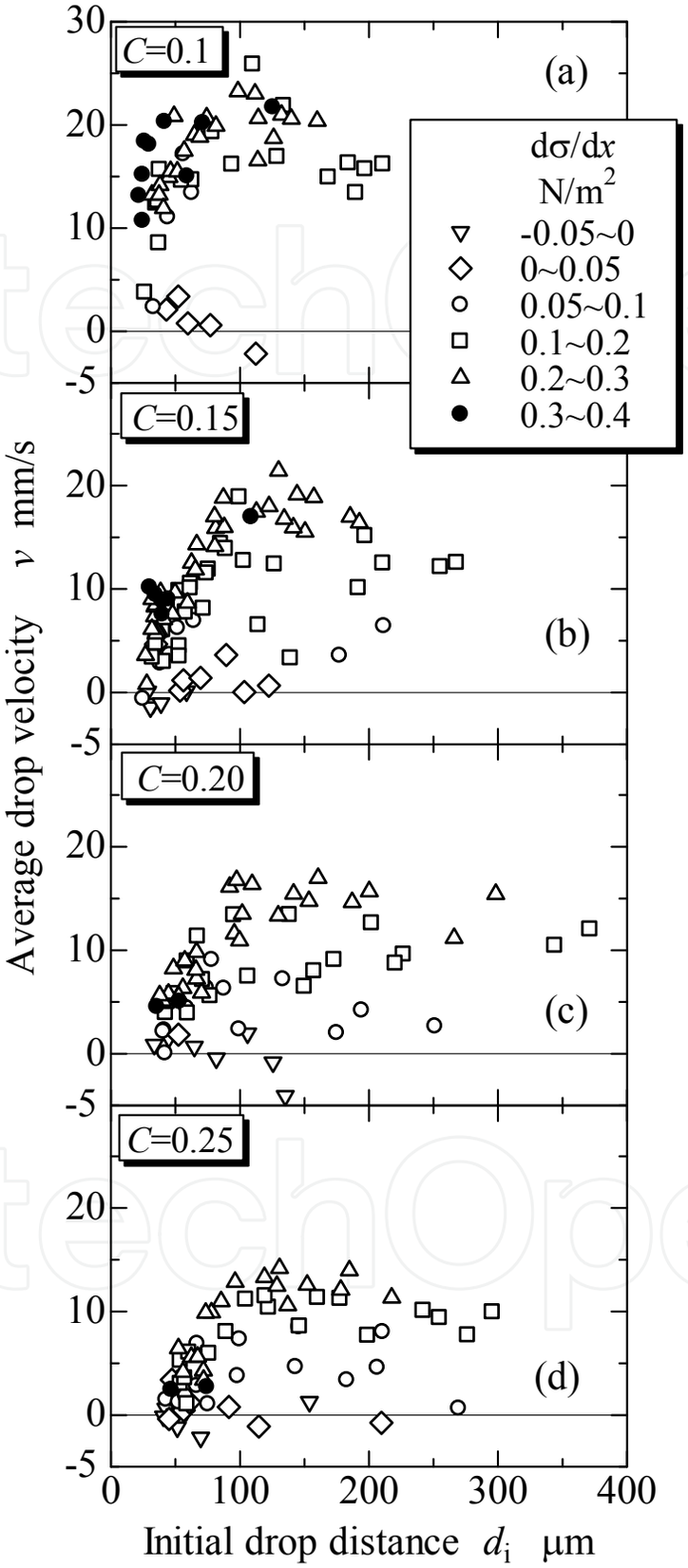

Figure 17. Variation of average drop velocity as a function of initial drop distance for various ethanol mass fractions and bulk surface tension gradients

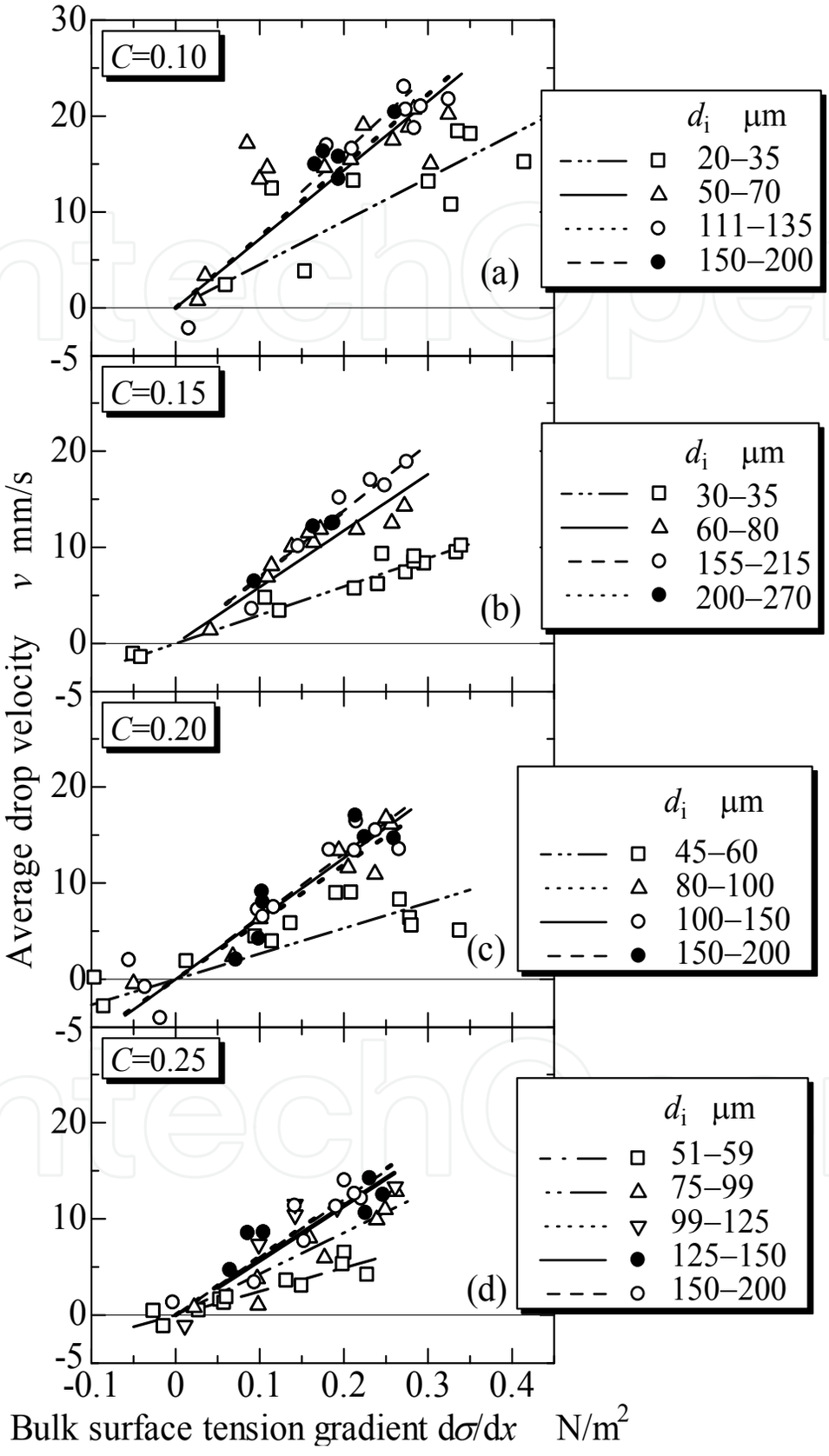

Figure 18. Variation of average drop velocity as a function of bulk surface tension gradient for various ethanol mass fractions and initial drop distances

3.5. Mechanisms of condensate drop movement

Experimental studies on the characteristics (effects of several parameters) of drop movement under a bulk temperature gradient on a heat transfer surface have been conducted for Marangoni dropwise condensation of water-ethanol vapor. However, the essential factor relating to Marangoni dropwise condensation and the condensate drop movement, the Marangoni force, cannot be experimentally measured. Therefore, to better understand the relationship between the Marangoni force and condensate drop movement, numerical simulation of the spontaneous movement of condensate drops was conducted using the volume of fluid (VOF) method. In this section, the 3-dimensional phenomenon of condensate drop movement was simulated using a 2-dimensional calculation in the domain presented in Fig. 19; therefore, only qualitative discussion is presented in this section.

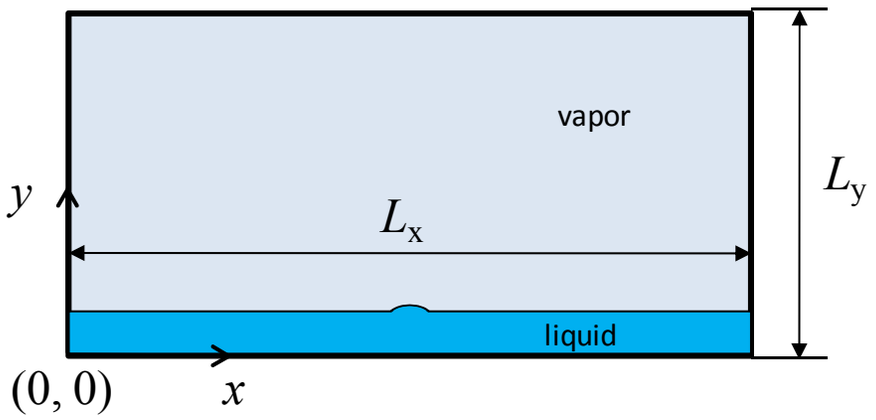

Figure 19. Calculation domain used for the numerical simulation

3.5.1. Governing equations

3.5.1.1. Liquid phase

In the calculation, the liquid phase was treated as incompressible. The continuity, momentum, and energy equations were solved.

$$\frac{\partial u_{\mathrm{L}}}{\partial x}+\frac{\partial v_{\mathrm{L}}}{\partial y}=0 \tag{1}$$

$$\frac{\partial u_{\mathrm{L}}}{\partial t}+u_{L}\frac{\partial u_{\mathrm{L}}}{\partial x}+v_{L}\frac{\partial u_{\mathrm{L}}}{\partial y}=g_{x}-\frac{1}{\rho_{L}}\frac{\partial P}{\partial x}+\upsilon_{L}\left(\frac{\partial^{2}u_{\mathrm{L}}}{\partial x^{2}}+\frac{\partial^{2}u_{\mathrm{L}}}{\partial y^{2}}\right) \tag{2}$$

$$\frac{\partial v_{\mathrm{L}}}{\partial t}+u_{\mathrm{L}}\frac{\partial v_{\mathrm{L}}}{\partial x}+v_{\mathrm{L}}\frac{\partial v_{\mathrm{L}}}{\partial y}=g_{y}-\frac{1}{\rho_{\mathrm{L}}}\frac{\partial P}{\partial y}+\upsilon_{\mathrm{L}}\left(\frac{\partial^{2}v_{\mathrm{L}}}{\partial x^{2}}+\frac{\partial^{2}v_{\mathrm{L}}}{\partial y^{2}}\right) \tag{3}$$

$$\frac{\partial T_{\mathrm{L}}}{\partial t}+u_{\mathrm{L}}\frac{\partial T_{\mathrm{L}}}{\partial x}+v_{\mathrm{L}}\frac{\partial T_{\mathrm{L}}}{\partial y}=\frac{\lambda_{\mathrm{L}}}{\rho_{\mathrm{L}}C_{\mathrm{P,L}}}\left(\frac{\partial^{2}T_{\mathrm{L}}}{\partial x^{2}}+\frac{\partial^{2}T_{\mathrm{L}}}{\partial y^{2}}\right) \tag{4}$$

$$\frac{\partial C_{\mathrm{L}}}{\partial t}+u_{\mathrm{L}}\frac{\partial C_{\mathrm{L}}}{\partial x}+v_{\mathrm{L}}\frac{\partial C_{\mathrm{L}}}{\partial y}=D_{\mathrm{L}}\left(\frac{\partial^2 C_{\mathrm{L}}}{\partial x^2}+\frac{\partial^2 C_{\mathrm{L}}}{\partial y^2}\right) \tag{5}$$

$$\frac{\partial F}{\partial t}+\frac{\partial u_{\mathrm{L}}F}{\partial x}+\frac{\partial v_{\mathrm{L}}F}{\partial y}=0. \tag{6}$$

3.5.1.2. Vapor phase

In the vapor phase, the vapor velocity in the y-direction was determined by the condensation rate at the vapor-liquid interface, and the vapor velocity in the x-direction was ignored. The diffusion equation was solved based on the assigned vapor velocity. After the results of diffusion equation were obtained, the temperature of the vapor mixture was calculated from the mass fraction based on the vapor line in the relation of vapor-liquid equilibrium.

$$\rho_{\mathrm{V}}v_{\mathrm{V}}=\dot{m} \tag{7}$$

$$\frac{\partial C_{\mathrm{V}}}{\partial t}+v_{\mathrm{V}}\frac{\partial C_{\mathrm{V}}}{\partial y}=D_{\mathrm{V}}\left(\frac{\partial^2 C_{\mathrm{V}}}{\partial x^2}+\frac{\partial^2 C_{\mathrm{V}}}{\partial y^2}\right) \tag{8}$$

$$T_{\mathrm{V}}=f\left(C_{\mathrm{V}}\right). \tag{9}$$

3.5.1.3. Vapor-liquid interface

The velocity distribution at the vapor-liquid interface is calculated by taking account of the effect of the surface tension gradient (stress balance at the vapor-liquid interface). This was used as the velocity boundary condition of the liquid phase. The temperature and mass fraction of ethanol at the interface were calculated based on the vapor-liquid equilibrium, energy balance and mass balance.

Condensation rate:

$$\rho_{\mathrm{V}}v_{\mathrm{V}}=\dot{m} \tag{10}$$

Energy balance:

$$-\lambda_{\mathrm{L}}\frac{\partial T_{\mathrm{L}}}{\partial y}=\Delta h_{\mathrm{V}}\dot{m} \tag{11}$$

Mass balance:

$$\dot{m}_{\mathrm{E}}=\rho_{\mathrm{V}}D_{\mathrm{V}}\frac{\partial C_{\mathrm{V}}}{\partial y}+C_{\mathrm{V}}\dot{m} \tag{12}$$

Mass fraction of liquid in the cell at the interface:

$$C_{\mathrm{L}}=\frac{\dot{m}_{\mathrm{E}}}{\dot{m}} \tag{13}$$

Vapor-liquid equilibrium:

$$C_{\mathrm{V}} = f\left(T_{\mathrm{surf}}\right) \tag{14}$$

$$C_{\mathrm{L}} = f\left(T_{\mathrm{surf}}\right) \tag{15}$$

Relationship between the surface tension coefficient and concentration of the liquid:

$$\sigma = f\left(C_{\mathrm{L}}\right) \tag{16}$$

Increase of F caused by condensation:

$$\frac{\partial F}{\partial t} = \frac{1}{\rho_{\mathrm{L}}}\frac{\dot{m}}{\Delta y} \tag{17}$$

Stress balance at the vapor-liquid interface:

$$\left(P_{\mathrm{V}} - P_{\mathrm{L}} + \frac{\sigma}{R}\right)n_i = \left(-\tau_{\mathrm{L},ij}\right)n_k + \frac{\partial \sigma}{\partial x_i} \tag{18}$$

3.5.2. Boundary and initial conditions

Considering the real phenomenon and the computation time, the calculation is conducted in a relatively small region of 600×200 μm^2 (Fig. 19). The boundary conditions are summarized in Table 1. The boundary at y=0 is set as the condensing surface, and y=L_{y} is the steady temperature/concentration boundary. In addition, the boundary condition at x=0, L_{x} is the free inlet/outlet flow. A thin (1.5 μm) liquid film is set initially on the condensing surface. A tiny protuberance is also given in the center of the initial liquid film as a disturbance. During the calculation, a certain mass fraction of ethanol vapor and the corresponding vapor line temperature are assigned to the boundary of y=L_{y}, and the temperature gradient (the right side is set as the high-temperature side) was assigned directly to the condensing surface of y=0. During the calculation, a constant temperature was initially assigned to the condensing surface. After the temperature/concentration distribution in the calculation region became close to that for the actual phenomenon with elapse of time, the temperature gradient was applied to the condensing surface.

Furthermore, the basic equations were discretized using a staggered grid. The convective term was approximated by a 1st–order upwind difference and the diffusion term by 2nd–order central difference. Pressure was calculated implicitly. Other variables such as velocity, temperature and mass fraction were calculated explicitly. The velocity field in the calculation region was calculated using the SOLA method. In addition, the variations of F at the vapor-liquid interface were calculated using the donor-acceptor method.

$y = L_y$	$\partial u/\partial x = 0\ ,\ v = 0$	$T = T_0$	$C = C_0$
$y = 0$	$u = 0\ ,\ v = 0$	$T = T_w(x)$	$\partial C/\partial y = 0$
$x = 0$	$\partial u/\partial x = 0\ ,\ \partial v/\partial y = 0$	$\partial T/\partial x = 0$	$\partial C/\partial x = 0$
$x = L_x$	$\partial u/\partial x = 0\ ,\ \partial v/\partial y = 0$	$\partial T/\partial x = 0$	$\partial C/\partial x = 0$

Table 1. Summary of the boundary conditions employed for the numerical simulation

3.5.3. Calculation results and discussion

3.5.3.1. Variation of liquid film and shape of condensate drop

The calculation results for an ethanol mass fraction of C = 0.09 are shown in Figs. 20–23. The variation in the thickness of the condensate film and the form of the free surface are shown in Fig. 20. The condensate film became thicker over time. Several condensate drops formed and became larger on the condensing surface including the spot where the initial disturbance was located.

3.5.3.2. Angle of the condensate drop

Figure 21 shows a comparison of condensate drops forming on condensing surfaces with different surface subcooling (ΔT=6 and 10 K). Condensate drops with similar diameters were selected and the shape of the drops was compared. Developed condensate drops were investigated to avoid the influence of initial conditions. The condensate drop was higher for larger surface subcooling (ΔT = 10 K). Thus, the angle of the condensate drop becomes larger when the surface subcooling is larger, which is in agreement with the experimental results and indicates the condensate drop angle becomes larger because of the stronger Marangoni force.

3.5.3.3. Driving force of drop movement

To investigate the driving force of condensate drop movement, the momentum of condensate liquid pulled into a condensate drop by the Marangoni force around the periphery was calculated. In the two-dimensional simulation, the momenta on the high and low-temperature sides of a condensate drop were calculated. The qualitative relation between the drop movement and the imbalance of momentum in the horizontal direction is discussed. In addition, the momentum was calculated at the position where the condensate film around the periphery of a condensate drop is the thinnest (in the valley around the base of a condensate drop).

The experimental results obtained so far indicate that there is a large amount of scatter in the velocities and angles of condensate drops, due to the coalescence of drops or unstable temperature distributions near the periphery of drops. Similar to the experimental results, it is considered that the calculation results also vary significantly around the average values in the numerical simulation. Thus, to avoid the influence of adjacent condensate drops, the condensate drop formed in the vicinity of the center of a condensing surface (Fig. 20) was selected. Because it was considered that the characteristics of a relatively isolated condensate

drop in the numerical simulation is nearly equal to that of condensate drops in the experiments.

The aspects of growth and movement of a condensate drop after the temperature gradient was applied are shown in Fig. 22 for C=0.09 and ΔT =10 K. The crests of the condensate drops are indicated by open circles. In addition, the horizontal component of momentum at the high/low-temperature side of the condensate drop and the temperature difference of the liquid surface between the high- (right side) and low- (left side) temperature sides of the condensing surface (boundary condition) are shown in Figs. 23(a) and (b), respectively. The surface temperature of the condensate on the high-temperature side of the condensate drop is higher than that of the low-temperature side, and the horizontal momentum of the condensate liquid is larger on the high-temperature side than that on the low-temperature side.

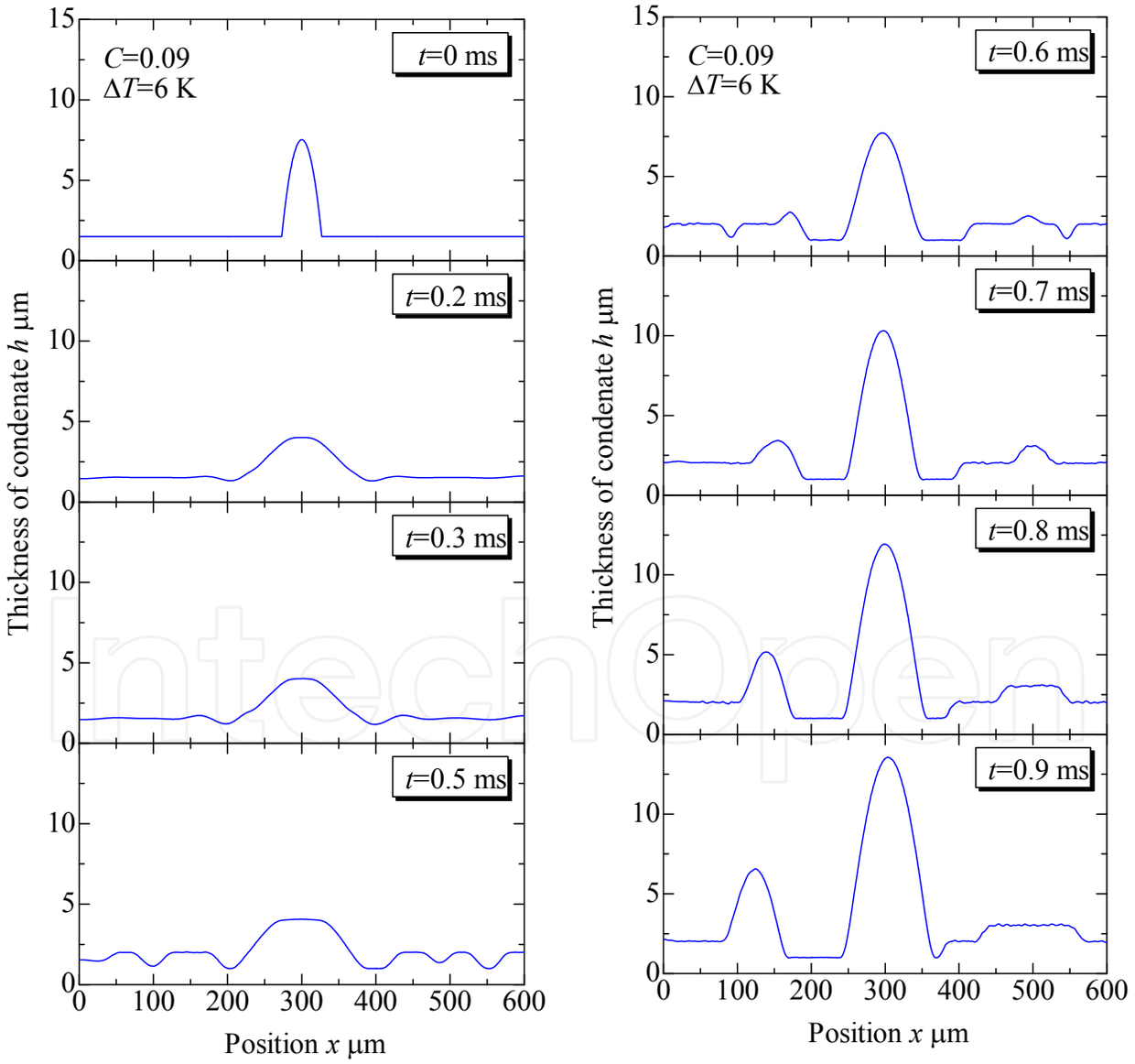

Figure 20. Variation of condensate liquid film thickness over time

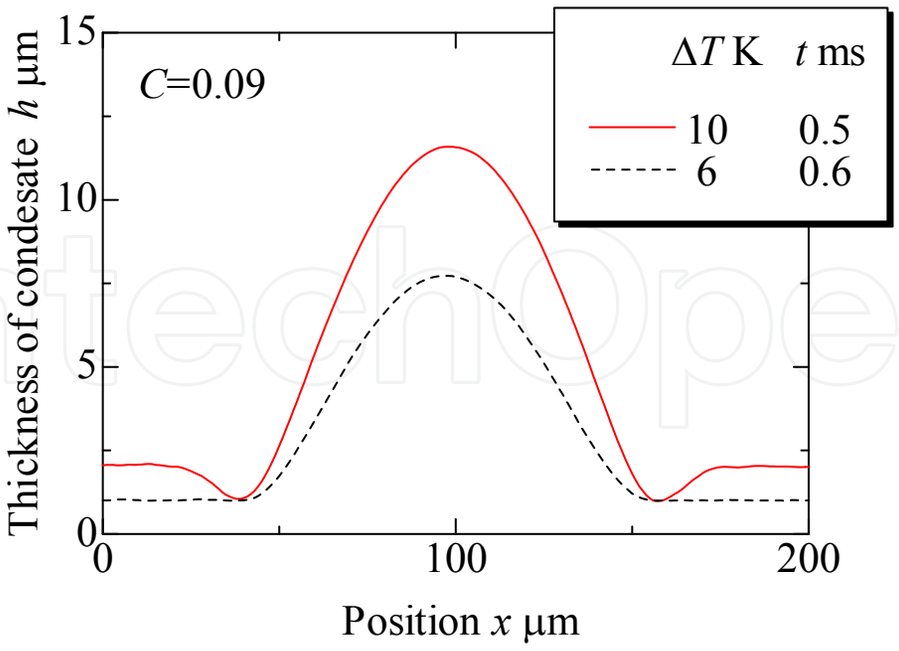

Figure 21. Comparison of condensate drop shape for different subcooling temperatures

These results correspond to those given in Fig. 22, where the growing condensate drop moves towards the high-temperature side. In conclusion, the condensate drop movement is in the direction of the side with the larger momentum of condensate liquid being pulled into the condensate drop by the Marangoni force. Thus, it could be inferred that an imbalance of the horizontal component of the Marangoni force is the driving force for condensate drop movement.

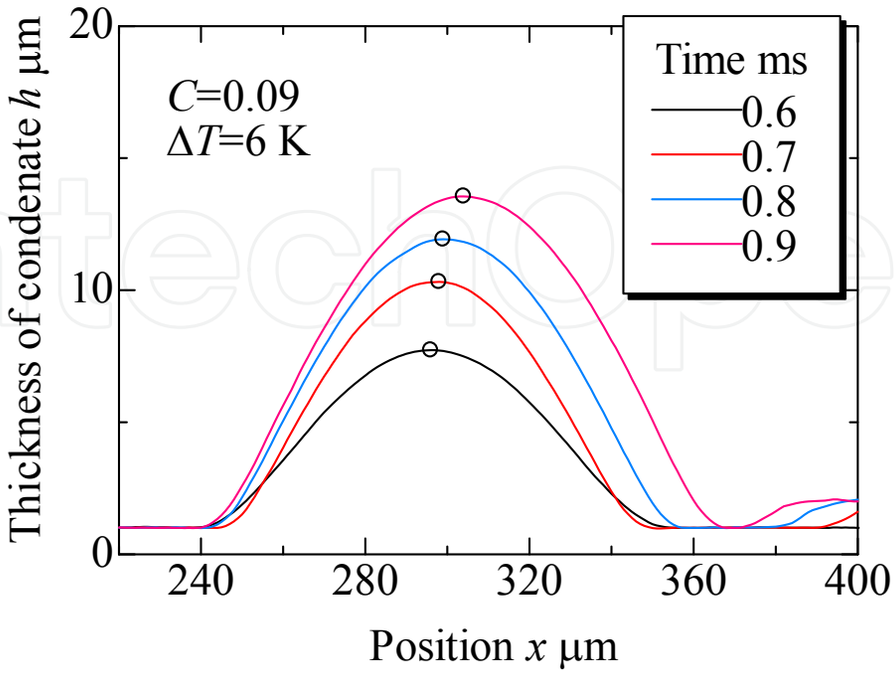

Figure 22. Growth and movement of a condensate drop over time

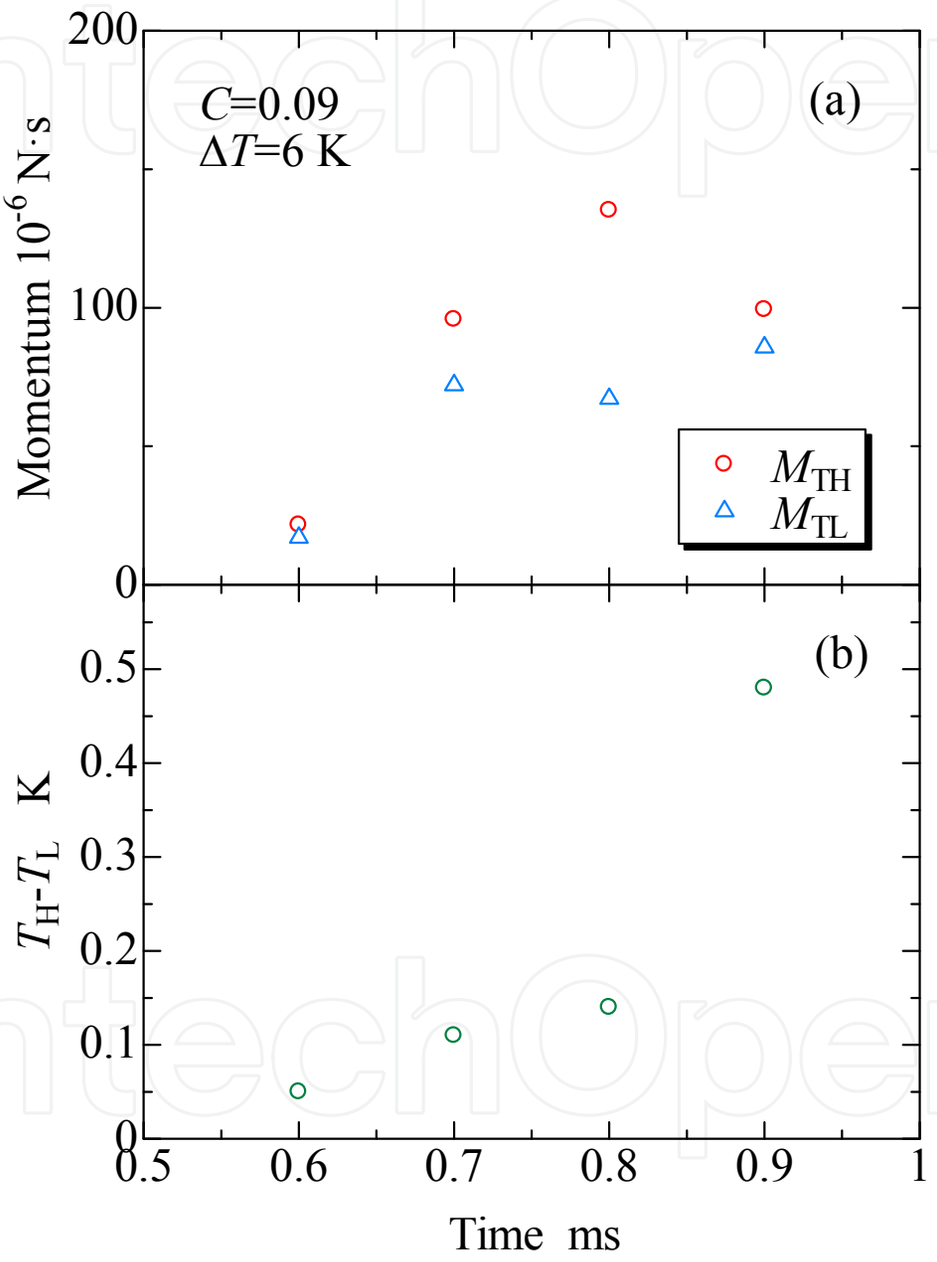

Figure 23. (a) Horizontal momentum of a condensate liquid driven into a condensate drop, and (b) surface temperature difference between the low- and high-temperature side of a condensate drop

4. Conclusion

Condensate drops move spontaneously on a heat transfer surface with a bulk temperature gradient in Marangoni dropwise condensation. It is conceivable that the velocity of a condensate drop is determined by the bulk surface tension gradient, Marangoni force, and the shape of the condensate drop. With a focus on these three factors, experimental and numerical studies were conducted on the spontaneous movement of condensate drops in the Marangoni condensation of a water–ethanol mixture. The results are summarized as follows:

1. Condensate drops move from the low-temperature to high-temperature side of a heat transfer surface. The velocity of condensate drop movement increases with the bulk surface tension gradient.
2. There are correlations among the Marangoni force, initial drop distance and angle of the condensate drop. It is appropriate to adopt the initial drop distance as a dominant parameter to express the characteristics of drop velocity.
3. When the initial drop distance decreases, the average drop velocity initially increases and then decreases after reaching a maximum at almost the same surface tension gradient. The average drop velocity increases linearly with bulk surface tension gradient for each initial drop distance range. The rate of increase in the drop velocity increases with the increasing initial drop distance.
4. Condensate drop movement is directed toward the side with a larger momentum of condensate liquid being pulled into the condensate drop by Marangoni force. It could be inferred that an imbalance of the horizontal component of Marangoni force is the driving force for condensate drop movement.

Nomenclature

C		Mass fraction of ethanol vapor
C_P	[J/kg·K]	Specific heat at constant pressure
D	[m²/s]	Diffusion coefficient
d	[mm]	Diameter of condensate drop
d_i	[μm]	Initial drop distance
F		VOF function, Force
g	[m/s²]	Gravity acceleration
Δh	[kJ/kg]	Latent heat
M	[N·s]	Momentum
$\dot{m}$	[kg/m²·s]	Mass flux of condensation
P	[kPa]	Pressure
T	[K]	Temperature

ΔT	[K]	Surface subcooling
t	[s]	Time
U	[m/s]	Velocity of vapor mixture
u	[m/s]	Horizontal velocity
v	[mm/s], [m/s]	Velocity of drop movement, Vertical velocity
x	[m]	Cartesian axis direction
y	[m]	Cartesian axis direction

Greek characters

α	[kW/m^{2}k]	Heat transfer coefficient
θ	[°]	Angle of condensate drop
σ	[mN/m]	Surface tension coefficient
δ	[μm]	Minimum condensate thickness
λ	[W/m·K]	Thermal conductivity
υ	[m^2/s]	Kinematic viscosity
ρ	[kg/m^3]	Density
τ	[Pa]	Shear stress

Subscripts

a	Advancing angle
r	Receding angle
surf	Vapor-liquid interface
E	Ethanol
L	Liquid phase, low-temperature side
V	Vapor phase
H	High-temperature side
x	Horizontal

Author details

Yoshio Utaka and Zhihao Chen
Division of Systems Research, Faculty of Engineering, Yokohama National University, Japan

5. References

[1] Mirkovich, V.V. and Missen, R.W. (1961). Non-Filmwise Condensation of Binary Vapor of Miscible Liquids, *Can. J. Chem. Eng.*, Vol. 39, pp. 86–87.

[2] Ford, J.D. and Missen, R.W., (1968). On the Conditions for Stability of Falling Films Subject to Surface Tension Disturbances; the Condensation of Binary Vapor, *Can. J. Chem. Eng.*, Vol. 48, pp. 309–312.

[3] Fujii, T., Osa, N. and Koyama, S., (1993). Free Convective Condensation of Binary Vapor Mixtures on a Smooth Horizontal Tube: Condensing Mode and Heat Transfer Coefficient of Condensate, *Proc. US Engineering Foundation Conference on Condensation and Condenser Design*, St. Augustine, Florida, ASME, pp. 171–182.

[4] Morrison, J.N.A. and Deans, J., (1997). Augmentation of Steam Condensation Heat Transfer by Addition of Ammonia, *Int. J. Heat Mass Transfer*, Vol. 40, pp. 765–772.

[5] Utaka, Y. and Terachi, N., (1995). Measurement of Condensation Characteristic Curves for Binary Mixture of Steam and Ethanol Vapor, *Heat Transfer-Japanese Research*, Vol. 24, pp. 57–67.

[6] Utaka, Y. and Terachi, N., (1995). Study on Condensation Heat Transfer for Steam–Ethanol Vapor Mixture (Relation between Condensation Characteristic Curve and Modes of Condensate), *Trans. Jpn. Soc. Mech. Eng.*, Series B, Vol. 61, No. 588, pp. 3059–3065.

[7] Utaka, Y. and Wang, S., (2004). Characteristic Curves and the Promotion Effect of Ethanol Addition on Steam Condensation Heat Transfer, *Int. J. Heat Mass Transfer*, Vol. 47, pp. 4507–4516.

[8] Utaka, Y. and Kobayashi, H., (2003). Effect of Vapor Velocity on Condensation Heat Transfer for Water–Ethanol Binary Vapor Mixture, *Proceedings of 6th ASME-JSME Thermal Engineering Conference*.

[9] Utaka, Y., (2011). Marangoni Condensation Heat Transfer. In: Belmiloudi, A., editor. Experimental Investigations and Industrial Systems, Heat Transfer-Theoretical Analysis, InTech. ISBN 978-953-307-226-5. pp. 327-350.

[10] Murase, T., Wang, H.S. and Rose, J.W., (2007). Marangoni condensation of steam-ethanol mixtures on a horizontal tube, *Int. J. Heat Mass Transfer*, Vol. 50, pp. 3774–3779.

[11] Hijikata, K., Fukasaku, Y. and Nakabeppu, O., (1996). Theoretical and Experimental Studies on the Pseudo-Dropwise Condensation of a Binary Vapor Mixture, *J. Heat Transfer*, Vol. 118, pp. 140–147.

[12] Akiyama, H., Nagasaki, T. and Ito, Y., (2001). A Study on the Mechanism of Dropwise Condensation in Water-Ethanol Vapor Mixture, *Thermal Science & Engineering*, Vol. 9, No. 6, pp. 19-27.

[13] Utaka, Y., Kenmotsu, T. and Yokoyama, S., (1998). Study on Marangoni Condensation (Measurement and Observation for Water and Ethanol Vapor Mixture), *Proceedings of 11th International Heat Transfer Conference*, Vol. 6, pp. 397–402.

[14] Utaka, Y. and Nishikawa, T., (2003). Measurement of Condensate Film Thickness for Solutal Marangoni Condensation Applying Laser Extinction Method, *J. Enhanc. Heat Transf.*, Vol. 10, No. 1, pp. 119–129.

[15] Utaka, Y. and Kamiyama, T., (2008). Condensate Drop Movement in Marangoni Condensation by Applying Bulk Temperature Gradient on Heat Transfer Surface, *Heat Transfer–Asian Research*, Vol. 37, No. 7, pp. 387-397.

[16] Chen, Z. and Utaka, Y., (2011). Characteristics of condensate drop movement with application of bulk surface temperature gradient in Marangoni dropwise condensation, *Int. J. Heat Mass Transfer*, Vol. 54, pp. 5049–5059.

IntechOpen